https://doi.org/10.20965/ijat.2011.p0377

Paper:

Identification of 5-Axis Machine Tools Feed Drive Systems for Contouring Simulation

Burak Sencer*, and Yusuf Altintas**

*Ultraprecision Engineering Laboratory, Nagoya University
Furo-cho, Chikusa-ku, Nagoya City, Aichi 464-8603, Japan
E-mail: burak@upr.mech.nagoua-u.ac.jp
**Manufacturing Automation Laboratory, University of British Columbia
2054-6250 Applied Science Lane Vancouver, B.C. V6T 1Z4 Canada
E-mail: altintas@mech.ubc.ca
[Received January 21, 2011; accepted March 9, 2011]

An identification technique is introduced for identifying closed loop transfer function of machine tool's feed drive systems to be used in simulation of the tracking and contouring performance of Computer Numerical Controlled (CNC) machine tools. The identification is performed from air-cutting tests utilizing only standard G-codes containing linear motion commands. A general transfer function model is derived for representing the closed loop tracking response of the feed drive system. The model considers the drive to be controlled by commonly used controller schemes such as P-PI Cascade, PID or the Sliding Mode Controller (SMC) with feed-forward dynamic and friction compensation. The parameters of the model transfer function are fitted to minimize the discrepancy between the actual and predicted axis position on the axis. In order to guarantee the stability of the identified model transfer function, bounds on the pole locations are imposed. The resultant constrained non-linear optimization problem is solved efficiently using the Particle Swarm Optimization (PSO) method. For achieving reliable convergence of the stochastic PSO algorithm, a parameter tuning strategy is presented. Simulation and experimental studies show that the identified feed drive model captures the fundamental dynamics of the drives system accurately for simulating their closed loop response. Combined with the kinematics of the machine, contouring errors of 5-axis CNC machine tools during simultaneous multi-axis motion are predicted.

Keywords: multi-axis control, CNC, identification, simulation, optimization

1. Introduction

Each drive on a commercial Computer Numerical Controlled (CNC) machine tool is controlled with feedback controllers. Commercial CNC drive control systems have generally closed and propriety architecture, and a detailed dynamic model including the controller is never provided to end-users. Therefore, an identification method is required to estimate the drive dynamics of a machine tool to simulate its overall tracking and contouring performance in virtual environment [1, 2]. This approach allows the end-user to predict the precision of their machine tools before they machine the actual part and hence improves the efficiency of the machining operation.

There has been extensive research in building models for feed drive systems, and identification of the drive parameters [3]. Most of those methods require disconnecting the feed drive system from the interpolator of the CNC system, and conducting a series of time identification tests that require use of rich excitation signals such as random sequence of step inputs or frequency domain identification tests [4, 5]. However, conducting such tests on a real CNC is not practical. It causes unwanted downtime and requires expertise in the identification area.

As an alternative, this paper presents an identification technique for identifying the closed loop transfer function of machine tool's feed drive system. The drive system is identified in closed loop, including the feed drive mechanism, motor amplifier, and the control law. A short Numerical Control (NC) Program i.e. G-code is used to excite the axis dynamics without interfering with the servo control loop [6]. The generalized drive model adapted from Erkorkmaz and Wong [7] is used to capture the key dynamics of the drive systems. In order to guarantee the stability of the identified transfer function of the drive models, bounds on the pole locations are imposed, and a constrained identification problem is constructed. The Particle Swarm Optimization (PSO) technique is then employed to solve the nonlinear optimization problem [8]. Simulation and experimental results demonstrate that the identified models can be used in estimating the tracking response of feed drive systems. Combined with the contouring models [9] the contouring performance of 5-axis CNC machine tools can be predicted.

2. Closed Loop Feed Drive Dynamics Model

This section presents the general closed loop model of modern 5-axis CNC drives controlled by various feedback

control techniques such as the P, PI, PID, P-PI cascade controllers with feed-forward dynamic and friction compensation.

The servo model shown in **Fig. 1a** considers the rigid body motion of a feed drive mechanism where J kgm^2 is the total inertia and B kgm^2/s is the viscous damping of the axis. In this model, motor and the amplifier are assumed to operate within their linear range, where u V is the control voltage command to the current amplifier modeled by a gain factor, K_a A/V, and the corresponding torque delivered to the drive is obtained by multiplying the current with the motor torque constant K_t A/V, and r_g mm/rad is transmission gain of the ball-screw mechanism.

The most commonly used position control structures in commercial CNC drives are shown in **Fig. 1b** and **c**. For instance, the P-PI controller scheme is illustrated in **Fig. 1b**. In this scheme, the velocity loop is closed using Proportional-Integral (PI) control by adjusting the gains K_p, K_i, and the position loop is closed by a proportional control (P) using K_v. The well known PID controller scheme is shown in **Fig. 1b**, where the position loop is directly closed using a Proportional-Integral-Derivative (PID) controller with gains K_p, K_i, K_d. In both of those controller schemes, the feed-forward compensation of axis dynamics is applied to widen the servo tracking bandwidth where $V_{ff} \in [0,1]$, $B_{ff} \in [0,1]$, $J_{ff} \in [0,1]$ are the respective gains used to cancel the dynamics in P-PI controller. Similarly, inertia and viscous friction feed-forward are implemented in the PID scheme to improve overall tracking performance. For both of the cases, the closed loop transfer function between the commanded (x_r mm) and the actual axis position (x mm) can be presented in the form of:

$$x(s) = \underbrace{\frac{b_0 s^2 + b_1 s + b_2 + a_3 \frac{1}{s}}{s^2 + a_1 s + a_2 + a_3 \frac{1}{s}}}_{G_{track}(s)} \cdot x_r(s) - \underbrace{\frac{\frac{r_g}{J}}{s^2 + a_1 s + a_2 + a_3 \frac{1}{s}}}_{G_{dist}(s)} \cdot d(s) \quad \ldots . \quad (1)$$

where $G_{track}(s)$ and $G_{dist}(s)$ are the equivalent axis tracking and disturbance transfer functions. In this model, the Coulomb friction, d is considered to be a strong source of contouring errors occurring during velocity reversals. Assuming that the friction values in positive (d^+) and negative (d^-) directions are close in the real system, the friction model can be expressed as:

$$d = \sin(\dot{x}) d_c \quad \ldots . \quad (2)$$

where d_c Nm is the average Coulomb friction torque, and $\sin(\dot{x})$ is the signum function that returns "1" when the axis velocity is positive, "-1" when the velocity is negative, and "0" otherwise. Substituting the friction model from Eq. (2) into Eq. (1) yields the generalized axis model as

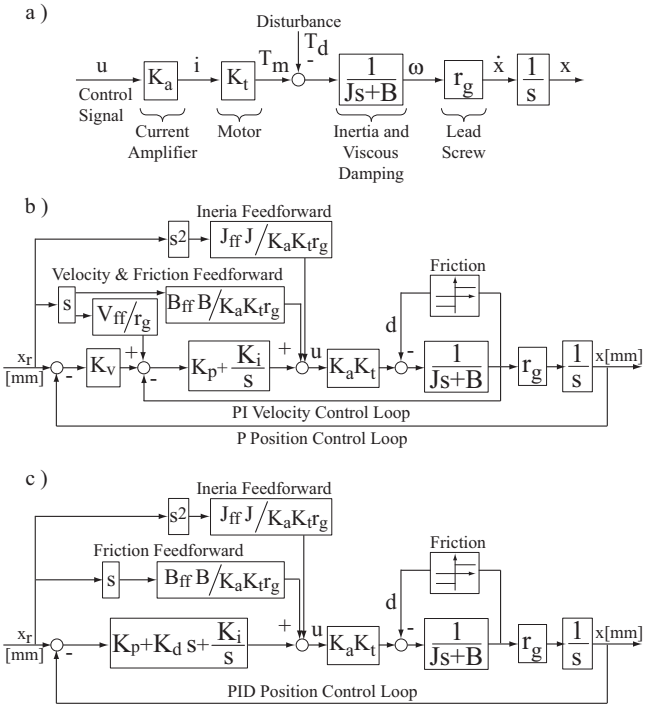

Fig. 1. Rigid body axis dynamics and commonly used CNC control structures.

$$\left[s^2 + a_1 s + a_2 + a_3 \frac{1}{s}\right] x(s) = \left[b_0 s^2 + b_1 s + b_2 + a_3 \frac{1}{s}\right] x_r(s) - \sin(\dot{x}) d_c. \quad (3)$$

For the P-PI controller structure, the model parameters are obtained as:

$$a_1 = \frac{B + K_a K_p K_t}{J},\ a_2 = \frac{K_a K_p K_v K_t r_g + K_a K_i K_t}{J},$$
$$a_3 = \frac{K_a K_i K_t K_v r_g}{J},$$
$$b_0 = I_{ff},\ b_1 = \frac{B B_{ff} + K_a K_p K_t V_{ff}}{J},$$
$$b_2 = \frac{K_a K_p K_v K_t r_g + K_a K_i K_t V_{ff}}{J},\ d_c = \frac{d r_g}{J} \quad . \quad (4)$$

and for the PID structure, the parameters become:

$$a_1 = \frac{B + K_a K_d K_t r_g}{J},\ a_2 = \frac{K_a K_p K_t r_g}{J},$$
$$a_3 = \frac{K_a K_t K_i r_g}{J},$$
$$b_0 = I_{ff},\ b_1 = \frac{B B_{ff} + K_a K_t K_d r_g}{J},\ b_2 = \frac{K_a K_p K_t r_g}{J},$$
$$d_c = \frac{d r_g}{J} \quad \ldots . \quad (5)$$

Hence, including the feed-forward dynamics compensation and the Coulomb friction, the model presented in Eq. (3) allows the closed loop dynamics of the axis drive to be presented with only a model consisting of 7 parameters; 3 poles (a_1, a_2, a_3), 3 zeros (b_0, b_1, b_2) and the average friction amplitude (d_c).

3. Identification of the Model Parameters

3.1. Objective Function

The objective is to identify the 7 parameters, a_1, a_2, a_3, b_0, b_1, b_2, d_c of the closed loop drive system to simulate the axis motion in virtual environment. The identification method is illustrated in **Fig. 2**. It is performed by executing a series of NC blocks of linear movements on the actual CNC machine tool to excite the closed loop drive dynamics as much as possible. In order to generate a high frequency excitation signal, the cubic acceleration profiling (i.e. "S-curve" functionality) should be disabled in the CNC controller, and the trapezoidal velocity profiling with unbounded jerk should be used instead. This helps the drive dynamics in higher frequencies to be captured by the linear model. The overall displacement range is varied from too short to long segments so that the performance of the drive for a wide range of feeds can be observed. The execution of several back and forth movements in different velocities allow the Coulomb friction amplitude to be identified more clearly. As the CNC follows the reference identification NC code, reference axis position and encoder measurements $(x_{r,k}, x_k)$ can be captured at the control loop period T_s, for a total of N samples on the fly. The 7 parameters can then be identified such that the error between the measured (x_k) and the predicted $(\hat{x}_k)$ axis motion is minimized in a Least Squares sense [9]:

$$\min f = \min \frac{1}{2} \sum_{k=1}^{N} (x_k - \hat{x}_k)^2. \quad \ldots\ldots\ldots (6)$$

From the real-time recorded reference and actual axis position $\left(x_{r,k}, x_k\right)$ on the CNC, the derivatives $\left(\dot{x}_k, \dot{x}_{r,k}, \ddot{x}_k, \ddot{x}_{r,k}\right)$ can be computed numerically, and the corresponding tracking errors are integrated numerically, $e_i = T_s \sum_{m=1}^{k} (x_{r,m} - x_m)$. Hence, the axis position is predicted by taking the inverse Laplace transform of Eq. (3) as

$$\hat{x}_k = \alpha_3 e_k - \alpha_1 \dot{x}_k - \alpha_2 \ddot{x}_k + \beta_0 x_{r,k} + \beta_1 \dot{x}_{r,k} + \beta_2 \ddot{x}_{r,k} - \text{sign}(\dot{x}_k)\delta \quad \ldots\ldots\ldots (7)$$

where the model parameters are normalized with respect to a_2,

$$\left.\begin{aligned} &\alpha_2 = 1/a_2,\ \alpha_1 = a_1/a_2,\ \alpha_3 = a_3/a_2 \\ &\beta_2 = b_0/a_2,\ \beta_1 = b_1/a_2,\ \beta_3 = b_3/a_2 \\ &\delta = d_c/a_2 \end{aligned}\right\}. \quad \ldots (8)$$

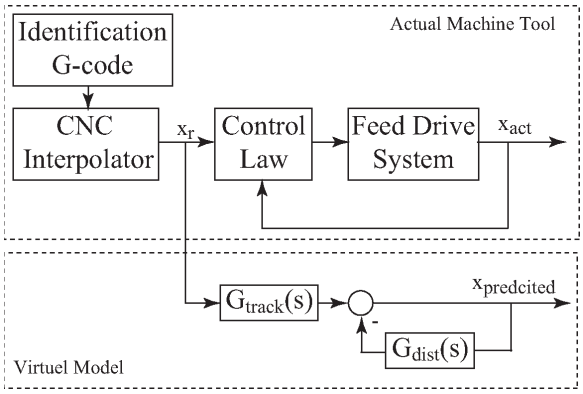

Fig. 2. Identification scheme.

The axis positions are stacked in the output vector $\mathbf{Y} = \begin{bmatrix} x_1 & x_2 & \ldots & x_N \end{bmatrix}^T$, and evaluating Eq. (7) for each sample, the predicted axis positions are written in a linear system of equation as:

$$\hat{x} = \begin{bmatrix} \hat{x}_1 \\ \hat{x}_2 \\ \vdots \\ \hat{x}_N \end{bmatrix} = \underbrace{\begin{bmatrix} e_1 & -\dot{x}_1 & -\ddot{x}_1 & -x_{r,1} & -\dot{x}_{r,1} & -\ddot{x}_{r,1} & \text{sign}(\dot{x}_1) \\ e_2 & -\dot{x}_2 & -\ddot{x}_2 & -x_{r,2} & -\dot{x}_{r,2} & -\ddot{x}_{r,1} & \text{sign}(\dot{x}_2) \\ \vdots & \vdots & \vdots & \vdots & \vdots & \vdots & \vdots \\ e_n & -\dot{x}_N & -\ddot{x}_N & -x_{r,N} & -\dot{x}_{r,N} & -\ddot{x}_{r,1} & \text{sign}(\dot{x}_N) \end{bmatrix}}_{\Phi} \underbrace{\begin{bmatrix} \alpha_3 \\ \alpha_1 \\ \alpha_2 \\ \beta_0 \\ \beta_1 \\ \beta_2 \\ \delta \end{bmatrix}}_{\Theta} \quad \ldots\ldots\ldots\ldots\ldots\ldots (9)$$

Finally, the objective function that minimizes the deviation of the predicted axis position $(\hat{x}_k)$ from the actual (x_k) be re-expressed using Eqs. (6) and (9) as:

$$\min_{\Theta} f = \min_{\Theta} \frac{1}{2} (\mathbf{Y} - \Phi\Theta)^{\mathbf{T}} (\mathbf{Y} - \Phi\Theta). \quad \ldots (10)$$

Hence, the set of parameters $(\mathbf{Y})$ that minimizes the objective function in Eq. (9) provides the model to predict the actual motion of the drive.

3.2. Stability Constraints

Most of the modern CNC controllers rely on feed-forward dynamic compensation to widen the tracking bandwidth and impose fast dynamics. Coulomb friction is another source of excitation injected to the system, which is usually compensated in the feed-forward loop. As a result, even though trapezoidal velocity profile is used in the CNC interpolator, the motion commands are relatively smooth and lack in persistence of excitation. Incorrect estimation of the drive parameters may occur, which results in unstable pole locations eliminating the practical use of the model presented above. As also addressed in [7], in

order to guarantee the stability of the identified transfer functions, bounds should be imposed on the poles of the identified transfer function model.

The pole locations of the general drive model from Eq. (3) can be computed as:

$$\begin{aligned} &s^3+a_1s^2+a_2s+a_3=(s+p)(s^2+2\zeta\omega_n s+\omega_n^2)\\ &p_1=-p,\ p_{2,3}=-\zeta\omega_n\pm j\omega_n\sqrt{1-\zeta^2} \end{aligned} \quad . \quad (11)$$

Stability of the identified model is achieved if all the poles are on the left hand side of the imaginary axis. Hence, lower and upper bounds on ζ, ω_n and the overdamped pole frequency p are imposed as constraints:

$$\left.\begin{aligned} &h_1: p-p_{\min}\geq 0\\ &h_2: \omega_n-\omega_{n,\min}\geq 0\\ &h_3: \zeta-\zeta_{\min}\geq 0\\ &h_4: \zeta-\zeta_{\max}\geq 0 \end{aligned}\right\}\Rightarrow \mathbf{h}\geq \mathbf{0} \quad . \ . \ . \ . \quad (12)$$

where $p_{\min}>0$, $\omega_{n,\min}>0$, and $\zeta_{\max}>\zeta_{\min}>0$. It should be noted that upper bound on $\zeta_{\max}$ is used to avoid the 3rd pole $\left(p_3=-\zeta\omega_n-j\omega_n\sqrt{1-\zeta^2}\right)$ from approaching to zero, and the allowable pole locations with the constraints are illustrated in **Fig. 3**. Hence, the objective function presented in Eq. (10) is constrained by Eq. (12) as:

$$\min_{\Theta}\frac{1}{2}(\mathbf{Y}-\Phi\Theta)^{\mathbf{T}}(\mathbf{Y}-\Phi\Theta) \text{ subjecto to: } \mathbf{h}\geq 0. \quad (13)$$

3.3. Solution Method

The augmented problem in Eq. (13) is a Linear Programming problem with non-linear constraints, and it is solved using the Particle Swarm Optimization (PSO) method as follows.

3.3.1. Principle of the PSO

Particle Swarm Optimization (PSO) algorithm is a population based intelligent search where individuals called as 'particles,' $\sigma_i=[\sigma_{i,1},\sigma_{i,2},\ldots,\sigma_{i,D}]^T$ containing the optimization variables$(1,...,D)$ that are essentially candidate solutions for a given optimization problem. Each particle's 'position,' i.e. the optimization variables assigned to that particle, is adjusted dynamically by the amount of $\mathbf{v}_i=(v_{i,1},v_{i,2},\ldots,v_{i,D})^T$, denoted as the particle's velocity. The PSO algorithm keeps track of each particle's history, and stores its best value, $\sigma_{i,pbest}$ that has minimized the objective function. Another best value that is tracked by the PSO minimizer is the overall best value of the entire particle batch obtained so far; $\sigma_{gbest}=\min(\sigma_{i,pbest})$, $i=1,\ldots,M$ where M is the total number of particles. Hence, the particles' position and velocity are adjusted at each iteration l with respect its own best location and the best location of the group as [8]:

$$\begin{aligned} &\mathbf{v}_i^{l+1}=w\cdot\mathbf{v}_i^l+\eta_1\left(\sigma_{i,pbest}^l-\sigma_i^l\right)+\eta_2\left(\sigma_{gbest}^l-\sigma_i^l\right)\\ &\sigma_i^l=\sigma_i^l+\mathbf{v}_i^{l+1}\\ &i=1,\ldots,M \end{aligned} \quad . \quad (14)$$

$\eta_1,\eta_2\in(0,2)$ are the learning gains that represent the weighting of the stochastic acceleration terms, which pulls each particle towards $\sigma_{i,pbest}$ and σ_{gbest}. Low learning values allow particles to search far from the target, and high values cause quick convergence with abrupt movement toward and past the optimum. w is called the inertia weight, and it controls the convergence behavior of the PSO. Hence, tuning of those parameters are crucial in achieving robust convergence from the PSO algorithm.

3.3.2. PSO Solution

In setting up the PSO to solve the optimization problem given in Eq. (13), the strategy is to conduct the search in terms of the closed loop pole frequency (ω_n,p) and damping (ζ) values instead of the model parameters directly. As shown in **Fig. 4**, the search region is bounded by the constraints expressed in Eq. (12), thus adopting this method simplifies the incorporation of stability constraints. Thus, each particle contains the optimization variables, namely the pole locations (ω_n,p) and the damping values(ζ) as:

$$\sigma_i=\left[p_i\ \omega_{n,i}\ \zeta_i\right]^T, i=1,\ldots,M. \quad . \ . \ . \ . \ . \quad (15)$$

As the particles sweep the bounded search region, the objective function,

$$f=\frac{1}{2}(\mathbf{Y}-\Phi\Theta)^{\mathbf{T}}(\mathbf{Y}-\Phi\Theta) \quad . \ . \ . \ . \ . \ . \ . \quad (16)$$

is evaluated. The parameter vector Θ is separated into two parts:

$$\Theta=\left[\underbrace{\alpha_3\ \alpha_1\ \alpha_2}_{\Theta_1}\underbrace{\beta_o\ \beta_1\ \beta_2\ \delta}_{\Theta_2}\right]^T=\left[\Theta_1\ \Theta_2\right]^T, \quad . \ (17)$$

and the particles (i.e. optimization variables) can be related to the first part of the drive parameters $\Theta_1=[\alpha_3\ \alpha_1\ \alpha_2]^T$ by using Eqs. (8) and (11) as:

$$\begin{aligned} &\alpha_3=\frac{a_3}{a_2}=\frac{p\omega_n^2}{\omega_n^2+2p\omega_n},\\ &\alpha_1=\frac{a_1}{a_2}=\frac{p+2p\omega_n}{\omega_n^2+2p\omega_n}, \quad . \ . \ . \ . \ . \ . \ . \quad (18)\\ &\alpha_2=\frac{1}{a_2}=\frac{1}{\omega_n^2+2p\omega_n}. \end{aligned}$$

In order to relate the particles to the remaining drive parameters $\Theta_2=[\beta_0\ \beta_1\ \beta_2\ \delta]^T$, the Least Squares subproblem [10] is constructed from Eq. (10). Upon the existence of $\left(\Phi_2^{\mathbf{T}}\Phi_2\right)^{-1}$, Θ_2 can be obtained uniquely from

$$\left[\Theta_1\ \Theta_2\right]\begin{bmatrix}\Theta_1\\ \Theta_2\end{bmatrix}=\mathbf{Y}\Rightarrow\Theta_2=\left(\Phi_2^{\mathbf{T}}\Phi_2\right)^{-1}\Phi_2^{\mathbf{T}}\left(\mathbf{Y}-\Phi_1\Theta_1\right).$$

$$. \ . \ . \ . \ . \ . \ . \ . \ . \ . \ . \ . \ . \ . \ . \ . \ . \quad (19)$$

By using only the pole frequency (ω_n,p) and damping (ζ) values as particle positions $(\sigma_i=[p_i\ \omega_{n,i}\ \zeta_i]^T)$, the objective function $\left(f=\frac{1}{2}(\mathbf{Y}-\Phi\Theta)^{\mathbf{T}}(\mathbf{Y}-\Phi\Theta)\right)$ is minimized by implementing the PSO algorithm as follows:

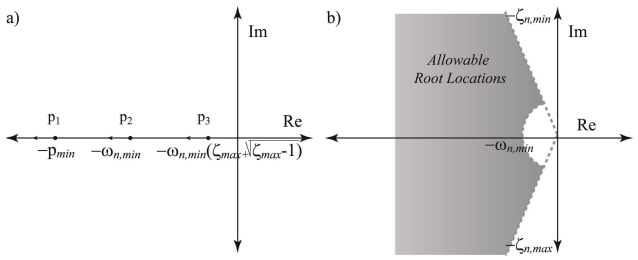

Fig. 3. Allowable locations for the real (a) and imaginary (b) poles.

Step 1. Specify the search region boundaries of the particles as $\sigma_{\min} = [p_{\min}\ \omega_{n,\min}\ \zeta_{\min}]^T$ and $\sigma_{\max} = [p_{\max}\ \omega_{n,\max}\ \zeta_{\max}]^T$ according to the constraints, and initialize each particle's position and velocity randomly as:

$$\left.\begin{aligned} \mathbf{v}_i^0 &= -\mathbf{v}_{\max} + 2r_1\mathbf{v}_{\max} \\ \sigma_i^0 &= \sigma_{\min} + r_2(\sigma_{\max} - \sigma_{\min}) \end{aligned}\right\} \quad \ldots . \quad (20)$$

where r_1 and r_2 are random numbers between 0 and 1 and $\mathbf{v}_{\max} = (\sigma_{\max} - \sigma_{\min}) \times (10\% \sim 20\%)$

Step 2. Evaluate the objective function f_i^l for each particle using Eqs. (16), (18) and (19).

Step 3. Find $f_{i,pbest}^l$ and compare it against f_i^l for each particle. If $f_i^l \le f_{i,pbest}^l$ then set $f_{i,best}^l = f_i^l$, and $\sigma_{i,pbest} = \sigma_i^l$.

Step 4. Search for the minimum value of f_i^l among all the particles, denote it as f_{gbest}^l, and set $\sigma_{gbest} = \sigma_i^l$.

Step 5. Check each particle individually, and if any value of ω_n, p and ζ is outside the search region, it is replaced within the closes bound as:

$$\begin{aligned} &\text{if } p_i^l < p_{\min} \Rightarrow p_i^l = p_{\min} \\ &\text{if } p_i^l > p_{\max} \Rightarrow p_i^l = p_{\max} \\ &\text{if } \omega_{n,i}^l < \omega_{n,\min} \Rightarrow \omega_{n,i}^l = \omega_{n,\min} \\ &\text{if } \omega_{n,i}^l > \omega_{n,\max} \Rightarrow \omega_{n,i}^l = \omega_{n,\max} \\ &\text{if } \zeta_i^l < \zeta_{\min} \Rightarrow \zeta_i^l = \zeta_{\min} \\ &\text{if } \zeta_i^l > \zeta_{\max} \Rightarrow \zeta_i^l = \zeta_{\max} \end{aligned} \quad \ldots . \quad (21)$$

Step 6. Return to the step 2 and iterate for the next particle position and velocity (σ_i^{l+1} and $\mathbf{v}_i^{l+1}$) using Eq. (14).

Step 7. When the number of iterations reaches the maximum the search algorithm is terminated, and the latest σ_{gbest} containing the optimal pole locations and damping values for the model is accepted. The model parameters(θ) are then computed from Eqs. (18), (19) and de-normalized by Eq. (8).

3.3.3. PSO Search Parameter Tuning

Although PSO is a stochastic algorithm, some guidance is required for selecting proper parameters to ensure convergence. The learning gains η_1, η_2 and the inertia weight w control the performance and convergence of the PSO algorithm [8]. Assuming that each particle contains only one element, $D = 1$ and during steady state the $\sigma_{i,gbest}$ and $\sigma_{i,pbest}$ values are constant, Eq. (14) can be re-written for each particle as:

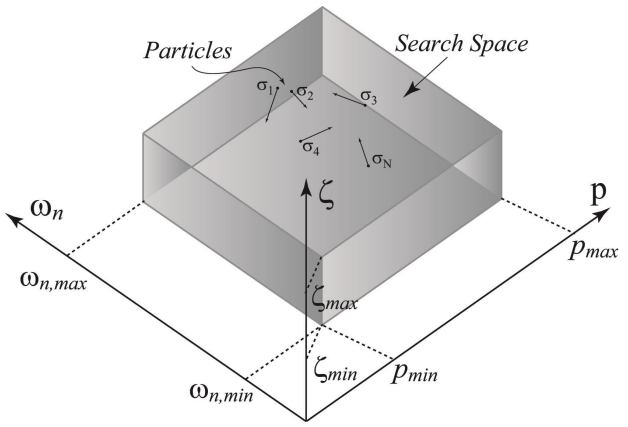

Fig. 4. Search region for the particle swarm optimization algorithm.

$$\underbrace{\begin{bmatrix} v_i^{l+1} \\ \sigma_i^{l+1} \end{bmatrix}}_{\mathbf{x}^{l+1}} = \underbrace{\begin{bmatrix} w & -\eta \\ w & 1-\eta \end{bmatrix}}_{\mathbf{H}} \cdot \underbrace{\begin{bmatrix} v_i^l \\ \sigma_i^l \end{bmatrix}}_{\mathbf{x}^l} + \underbrace{\begin{bmatrix} 1 \\ 1 \end{bmatrix}}_{\mathbf{B}} \underbrace{\left(\eta_1\sigma_{i,pbest}^l + \eta_2\sigma_{gbest}^l\right)}_{u}, \quad (22)$$

and $\eta = \eta_1 + \eta_2$.

By doing so, Eq. (22) models evaluation of the particle as a discrete linear dynamic system in state space form. $\mathbf{x}^l = [v_i^l\ \sigma_i^l]^T$ is the state vector, $\mathbf{B} = [1\ 1]^T$ is the input matrix and $u = \eta_1\sigma_{i,pbest}^l + \eta_2\sigma_{gbest}^l$ is the constant input. Hence, one can ensure the stability of the discrete PSO model by setting the Eigenvalues of the state matrix $\mathbf{H}$ within the unit circle [10]. The characteristic equation can be calculated as:

$$\det(\lambda\mathbf{I} - \mathbf{H}) = \lambda^2 + (\eta - w - 1)\lambda + w, \quad \ldots (23)$$

and the roots are:

$$\lambda_{1,2} = \left\{ \begin{array}{l} \left[\ (w+1-\eta) \pm \sqrt{\Delta}\ \right]/2,\ \Delta \ge 0 \\ \left[\ (w+1-\eta) \pm j\sqrt{-\Delta}\ \right]/2, \Delta < 0 \end{array} \right\}, \quad (24)$$

$$\Delta = (\eta - 1)^2 - 2w(\eta + 1) + w^2.$$

The objective is to set proper tuning parameters to ensure convergence of the PSO algorithm. It should be noted that, tuning the algorithm for the fastest convergence is not studied in this context. But, the following fundamental observations give a quick guidance in selecting the PSO parameters so that reliable convergence is achieved. According to Eq. (24) when $\Delta < 0$, the $\lambda_{1,2}$ are complex conjugate, and their norm become $\|\lambda_1\| = \|\lambda_2\| = \sqrt{w} < 1$. Therefore, setting $w \in (0,1)$ ensures the convergence of PSO. The following conditions from Eq. (24) give de-

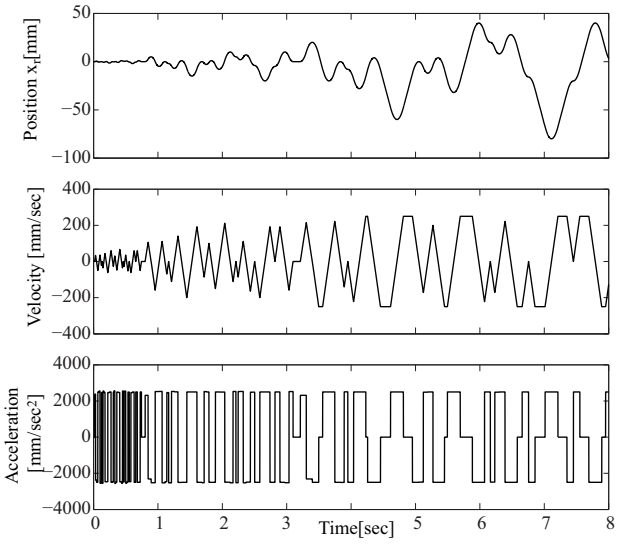

Fig. 5. Identification G-code trajectory send to each drive.

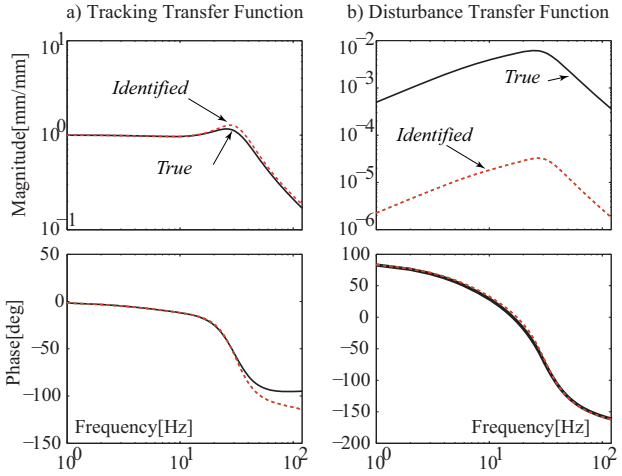

Fig. 6. True and identified transfer functions for the P-PI controlled virtual drive.

Table 1. True and identified closed loop parameters for the P-PI controlled virtual drive.

Search Variables	Actual	PSO Estimate
ω_n[Hz]	30.6	31.3
ζ[]	0.45	0.39
p[Hz]	10.8	11.4
Model Parameters	**Actual**	**PSO Estimate**
a_1	238.4335	226.94681
a_2	48421.5859	49915.0545
a_3	2.487140.30	2778130.868
b_0	0	-0.05340
b_1	117.5424	104.366781
b_2	37258.9796	37446.2295
d_c	2.6815	585.31

tailed insight on the conditions for the convergence:

1. When $\eta = 0$, $\lambda_1 = 1$, $\lambda_2 = w$, and the PSO is at the border of convergence or divergence.
2. When $\eta = 1$, $\Delta = w^2 - 4w < 0$, and for $w \in (0,1)$ PSO converges.
3. When $\eta = 2$, $\Delta = w^2 - 6w + 1 = (w-3)^2 - 8$ and for $w \in (0.172, 1)$, $\Delta < 0$ PSO converges.
4. When $\eta = 3$, $\Delta = w^2 - 8w + 14 = (w-4)^2 - 12$ and for $w \in (0.536, 1)$, $\Delta < 0$ and PSO converges.
5. When $\eta = 4$, $\Delta = w^2 - 10w + 9 = (w-5)^2 - 16 > 0$ and $\lambda_2 = \left[(w-3) - \sqrt{\Delta}\right] \Big/ 2 < -1$ results in divergence.

As a conclusion, the learning gains can be selected as $\eta_1 + \eta_2 = \eta \in (0,3)$, and the weight factor in the interval of $w \in (0.6, 1)$ ensures convergence of the PSO.

4. Simulation and Experimental Results

The effectiveness of the identification strategy is verified in both simulation and experimental case studies. The identification G-code is shown in **Fig. 5**. The G-code consists of 70 random linear movements commanded within the range of ± 50 mm with a maximum feedrate of 250 mm/sec and 2500 mm/sec^2 acceleration. Due to the short distance between the position commands, the desired velocity is not necessarily reached, which allows the drive response to be observed for a wider velocity range. Trapezoidal velocity profiling is used to ensure good persistence in the excitation signal, and the reference and actual position commands are collected at a sampling period of $T_s = 1$ msec.

In applying the PSO optimization method, the search space is bounded by $\omega_{n,\min} = p_{\min} = 0.2$ Hz, $\omega_{n,\max} = p_{\max} = 500$ Hz, $\zeta_{n,\min} = 0.2$ and $\zeta_{n,\max} = 2.0$. The weights are set to $\eta_1 = 0.103$, $\eta_2 = 2.897$ and $w = 0.6$. The number of particles is limited to $M = 200$, and the number of maximum iteration is set to 100.

4.1. Validation on a Virtual Drive

The identification strategy was first evaluated on a P-PI cascade controlled virtual drive system. The true and PSO estimated closed loop parameters are summarized in **Table 1**. As noted, there is slight discrepancy between the true and the PSO estimated drive parameters. The slower pole at 10.8 Hz is estimated at 11.4 Hz, and the complex conjugate poles at 30.6 Hz are estimated at 31.3 Hz. A comparison between the true and estimated tracking and disturbance Frequency Response Functions (FRF) is presented in **Fig. 6**.

Considering the true and predicted FRF's, the identified tracking transfer function is in good agreement up to 30 Hz, which is within the tracking range of most CNC motion systems. Furthermore, noted from the phase match, the disturbance transfer function is also in good agreement. There is $221\times$ difference between the DC amplitudes of the disturbance transfer function, which actually compensates for the discrepancy between the true and the estimated Coulomb friction (d_c) given in **Table 1**.

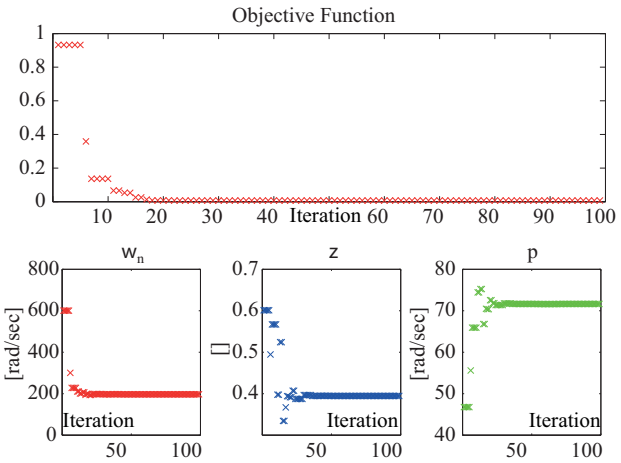

Fig. 7. PSO parameter convergence.

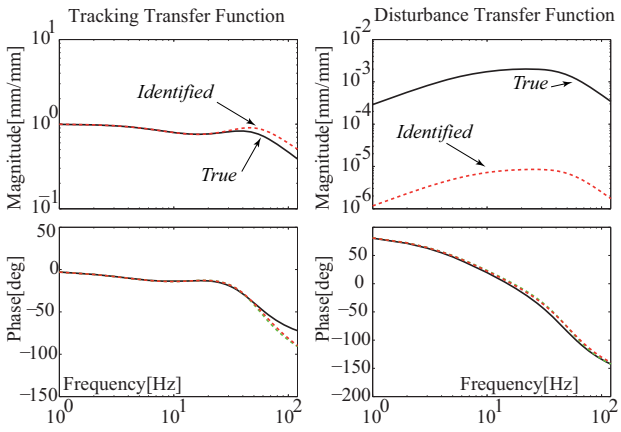

Fig. 8. True and identified transfer functions for the PID controlled virtual drive.

Table 2. True and identified closed loop parameters for the PID controlled virtual drive.

Search Variables	Actual	PSO Estimate
ω_n[Hz]	30.6	31.3
ζ[]	0.45	0.39
p[Hz]	10.8	11.4
Model Parameters	**Actual**	**PSO Estimate**
a_1	238.4335	226.94681
a_2	48421.5859	49915.0545
a_3	2.487140.30	2778130.868
b_0	0	-0.05340
b_1	117.5424	104.366781
b_2	37258.9796	37446.2295
d_c	2.6815	585.31

In overall, the drive identification is successful in capturing the key dynamic characteristics required to predict the tracking performance of the actual drives. **Fig. 7** shows the convergence of the PSO. As noted, the parameters converge to their steady state values well within 100 iterations resulting in rapid solution to the identification problem.

The second identification test is performed on a PID controlled virtual drive system, and the estimated drive parameters are summarized in **Table 2**. As noted, there is a close match between the actual and identified drive parameters on the PID controlled drive. This can also be verified from the FRFs presented in **Fig. 8**. The tracking transfer functions are again in good agreement up to 50 Hz ensuring accurate prediction of drive position from the identified model.

4.2. Validation on a Ball Screw Drive

After the identification algorithms have been tested on the virtual drive, they are evaluated experimentally on a ball screw driven table. The experimental ball-screw table is shown in **Fig. 9**. The closed loop control is implemented using the Dspace Digital Signal Processing (DSP) [11] system at 1 kHz where the motor position is measured form the rotary encoder, and the torque command is send to the amplifier, which operates in the torque mode. First, the P-PI control algorithm is implemented on the experimental setup, and the identification procedure is applied to fit the model parameters. Once the model parameters are obtained from the rapid identification procedure, validation toolpath is interpolated using trapezoidal trajectory with 250 mm/sec cruise velocity and acceleration of 2500 mm/sec^2 to compare predicted position to the actual drive position. The tracking result of P-PI controller during the validation run is presented in **Fig. 10a**. The true axis tracking errors on the drive are measured in the range of 400 μm, and the identified model predicts axis position with a maximum prediction discrepancy of 20 μm validating effectiveness of the proposed identification.

A robust Sliding Mode Control (SMC) scheme [12] has also been implemented to test the performance of the identification algorithm. The SMC cancels out inertia and friction completely to widen up the position bandwidth resulting in much faster dynamics that are more difficult to be excited. As shown in **Fig. 10b**, the tracking errors for SMC system are in the range of 40 μm, and some chattering is observed in the tracking response. The identified model still captures the general drive response under the SMC. In addition, as noted from the velocity transverses, the disturbance transfer function is also identified well enough. It should also be noted that when the stability constraints are not included in the PSO, the identification procedure has produced unstable models due to aggressive pole zero cancellations in the sliding mode controller structure. Thus, proposed identification method can be used in estimating systems with wide tracking bandwidths that are difficult to excite.

4.3. Validation on a Virtual 5-Axis Machine Tool

At last, the rapid identification technique has been tested on a virtual 5-axis machine tool for predicting the contouring errors during 5-axis machining. Contouring errors on a 5-axis machine tool can be defined as the

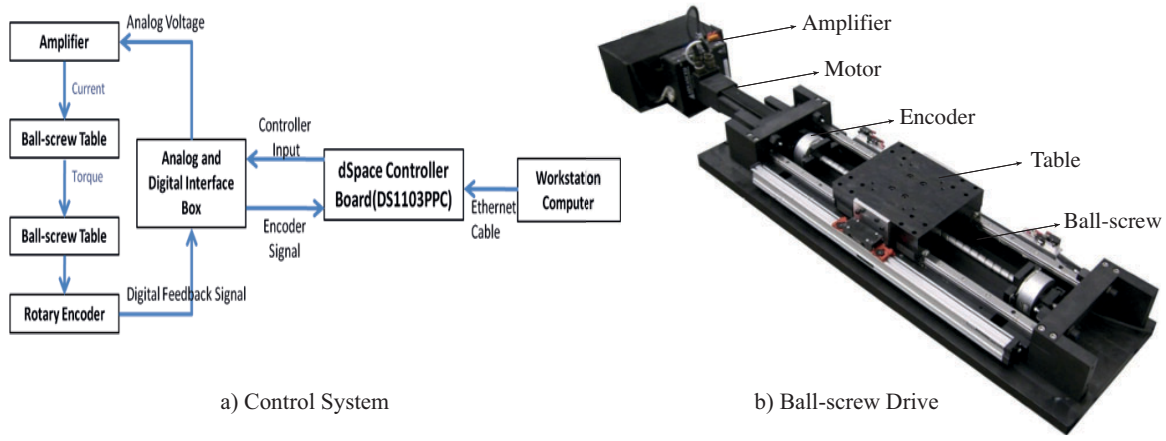

a) Control System b) Ball-screw Drive

Fig. 9. Experimental setup a) control system and b) ball-screw drive setup.

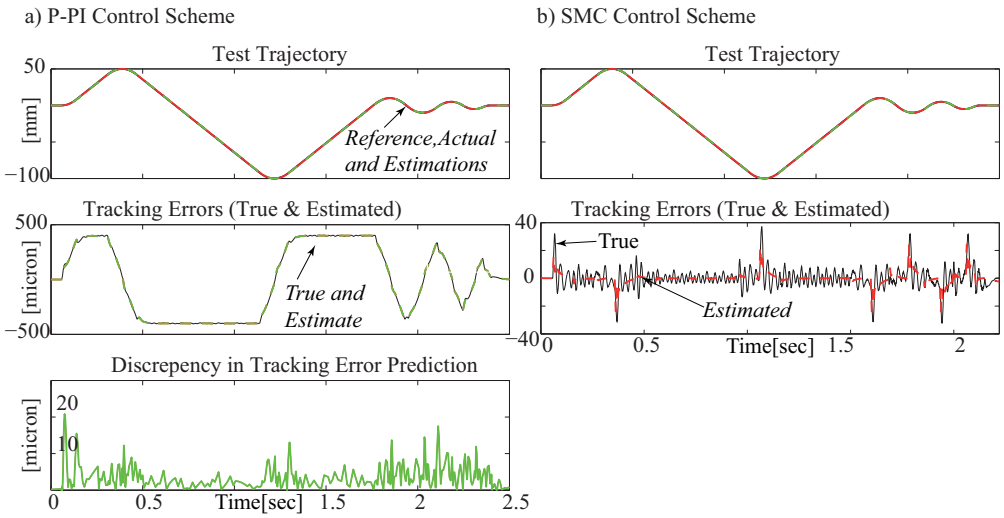

Fig. 10. Estimated and experimentally verified tracking performance of P-PI (a) and SMC (b) controlled drive.

Table 3. True and identified closed loop parameters for the P-PI controlled virtual 5-axis macihine tool drive parameters.

		Actual				
		X	**Y**	**Z**	**A**	**C**
Search Variables	ω_n[Hz]	55.54	73.5	73.6	31.9	27.3
	ζ[]	0.39	0.27	0.28	0.47	0.57
	p[Hz]	19.3	22.12	22.2	9.29	8.45
PSO Estimated						
Search Variables	ω_n[Hz]	58	90.9	138.5	24.19	68.9
	ζ[]	0.27	0.2	2	1.53	2
	p[Hz]	20.12	24.5	-138.5	24.19	68.9

normal deviation of the tool tip position from the reference toolpath [9]. In other words, contouring errors represent the actual part errors left on the part surface, and can be computed by combining both kinematics of the 5-axis CNC and the dynamic model of individual drives. In order to simulate the contouring performance, kinematic model of the Mori Seiki NMV5000 machining center is used. Corresponding forward and inverse kinematics solutions for this rotary tilting table 5-axis machine tool are adopted from [13]. The contouring error model for 5-axis machining is utilized from the literature [9], and dynamics of individual drives is then identified using the proposed technique. P-PI cascade controllers with feed-forward dynamics compensation are designed for each motion axis on a 5-axis machine tool. The identification procedure is applied on each drive, and identified drive parameters are presented in **Table 3**.

A spiral tool-path, shown in **Fig. 11a**, is interpolated with a tangential velocity of 75 mm/sec and acceleration of 1500 mm/sec^2 to achieve simultaneous motion of all the axes. The tracking errors of the drives are computed from identified models and the contouring errors are computed from reference and actual drive positions as described in [9]. **Fig. 11b** shows the true and estimated contour errors. The contouring errors computed from the true and identified model responses are in very good match. The discrepancy between the estimated and true contour errors is observed to be less than 10 μm, which validates the effectiveness of the identification method to be used in 5-axis contouring error prediction.

a) 5-Axis Contouring ToolPath

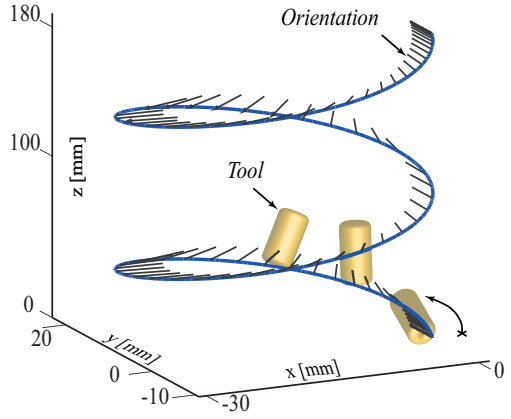

b) True and Estimated Contouring Errors

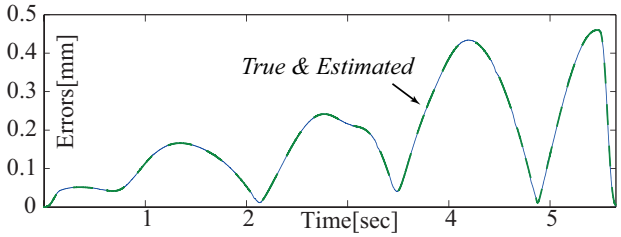

Fig. 11. True and estimated contouring errors on a virtual 5-axis machine tool.

5. Conclusions

Closed loop dynamics of various CNC feed drive systems can be identified accurately with simple air cutting tests using the proposed technique. The pole-zero cancellations in the true system, and lack of excitation in the command signal generated by the CNC interpolator causes ordinary least squares solution to produce models with unstable poles. The proposed Particle Swarm Optimization solution accommodates stability constraints to tackle the problem, and stable identification of drive models is guaranteed. Hence, the identified drive model can directly be utilized in contouring simulation of 3-axis Cartesian machines. Combined with kinematic model, identified drive models also allow simulation of the contouring performance of commercial 5-axis CNC machine tools.

Acknowledgements

Mori Seiki NMV5000 is loaned by the Machine Tool Technologies Research Foundation (MTTRF). The research is funded by NSERC and Pratt & Whitney Canada chair and AUTO21 grants.

References:

[1] Y. Altintas, C. Brecher, M. Weck, and S. Witt, "Virtual Machine Tool," Annals of CIRP, 54/1, pp. 651-673, 2005.

[2] K. Erkorkmaz, Y. Altintas and C.-H. Yeung, "Virtual computer numerical control system," Annals of CIRP 55/1, pp. 399-402, 2006.

[3] R. Sato and M. Tsutsumi, "Modeling, and Controller Tuning Techniques for Feed Drive Systems," Proc. of the ASME-IMECE'05, Orlando, FL, IMECE2005-80596, 2005.

[4] E. D. Tung and M. Tomizuka, "Feed-Forward Tracking Controller Design Based on the Identification of Low Frequency Dynamics," J. of Dynamic Systems Measurement and Control – Trans. of the ASME, Vol.115, Issue 3, pp. 348-356, 1993.

[5] K. Erkorkmaz and Y. Altintas, "High Speed CNC System Design: Part II – Modeling and Identification of Feed Drives," Int. J. of Machine Tools & Manufacture, Vol.41, Issue 10, pp. 1487-1509, 2010.

[6] Y. Altintas and B. Sencer, "Identification of 5-Axis Machine Tool Feed Drive Systems for Contouring Simulation," 4th CIRP Int. Conf. on High Performance Cutting, Gifu-Japan, 24-26 October, 2009.

[7] K. Erkorkmaz and W. Wong, "Rapid Identification Technique for Virtual CNC Drives," Int. J. of Machine Tools & Manu, Vol.47, pp. 1381-1392, 2007.

[8] R. C. Eberhart and J. Kennedy, "A New Optimizer Using Particle Swarm Theory," Proc. of 6th Int. Symp. on Micromachine Human Sci., Vol.1, pp. 39-43, 1995.

[9] B. Sencer, Y. Altintas, and E. A. Croft, "Modeling and Control of Contouring Errors for Five-Axis Machine Tools. Part I – Modeling," Trans. of ASME J. of Manu. Science and Eng., Vol.131, Issue 3, 031006, 2009.

[10] L. Ljung, "System Identification: Theory for the User," Prentice-Hall Of Canada Ltd., Englewoods Cliffs, NJ, 1998.

[11] dSPACE GmbH, www.dspace.com.

[12] Y. Altintas, K. Erkorkmaz, and W.-H. Zhu, "Sliding Mode Controller Design for High-Speed Drives," Annals of CIRP 49/1, pp. 265-270, 2000.

[13] O. R. Tutunea-Fatan and H. Y. Feng, "Configuration analysis of Five-Axis Machine Tools Using a Generic Kinematic Model," Int. J. of Machine Tools and Manufacture, Vol.44, No.11, pp. 1235-1243, 2004.

Name:
Burak Sencer

Affiliation:
JSPS Scholar, Post Doctoral Researcher at the Ultraprecision Engineering Laboratory (UPR) of the Nagoya University

Address:
Nagoya University, Department of Mechanical Science and Engineering, Graduate School of Engineering, Building 2-204, Furo-cho, Chikusa-ku, Nagoya City, Aichi 464-8603, Japan

Brief Biographical History:

2003- Joined Manufacturing Automation Laboratories (MAL) of the University of British Columbia (UBC)
2005- Obtained Ma.Sc degree at UBC
2009- Obtained Ph.D degree at UBC
2010- Joined Ultra-precision Engineering Laboratories of Nagoya University

Main Works:

• B. Sencer and Y. Altintas, "Modeling and Control of Contouring Errors for Five-Axis Machine Tools. Part II – Precision Contour Controller Design," Trans. of ASME, J. of Manufacturing Science and Engineering, Vol.131, Issue 3, 031007, 2009.
• B. Sencer, Y. Altintas, and E. A. Croft, "Feed Optimization for Five-Axis CNC Machine Tools with Drive Constraints," Int. J. of Machine Tools and Manufacture, Vol.48, No.7-8, pp. 733-745, 2007.

Membership in Academic Societies:

• The Japan Society of Professional Engineers (JSPE)
• Japan Society for the Promotion of Science (JSPS)

Name:
Yusuf Altintas

Affiliation:
NSERC P&WC Chair Professor, Manufacturing Automation Laboratory, University of British Columbia, Mechanical Engineering Department

Address:
2054-6250 Applied Science Lane Vancouver, B.C. V6T 1Z4 Canada

Brief Biographical History:
Professor at the University of British Columbia since 1986.

Main Works:
• Metal cutting mechanics, machine tool vibrations, machine tool control.

Membership in Academic Societies:
• American Society of Mechanical Engineers (ASME)
• Society of Manufacturing Engineers (SME)
• International Academy of Production Engineering Researchers (CIRP)
• Canadian Academy of Engineers (CAE)
• Royal Society of Canada (RSC)